A Fast Numerical Algorithmus for Thermographic Diagnostics

K.F. Mast, H. Würz+

IPP 1/247 Juni 1989

MAX-PLANCK-INSTITUT FÜR PLASMAPHYSIK

8046 GARCHING BEI MÜNCHEN

MAX-PLANCK-INSTITUT FÜR PLASMAPHYSIK

GARCHING BEI MÜNCHEN

A Fast Numerical Algorithmus for Thermographic Diagnostics

K.F. Mast, H. Würz+

IPP 1/247 Juni 1989

+ Kernforschungszentrum Karlsruhe

Die nachstehende Arbeit wurde im Rahmen des Vertrages zwischen dem Max-Planck-Institut für Plasmaphysik und der Europäischen Atomgemeinschaft über die Zusammenarbeit auf dem Gebiete der Plasmaphysik durchgeführt.

A Fast Numerical Algorithmus For Thermographic Diagnostics

K.F. Mast and H.Würz+
Max-Planck-Institut für Plasmaphysik, EURATOM-Association, D-8046 Garching
+ Kernforschungszentrum Karlsruhe

Introduction

A simple and fast numerical method to evaluate the absorbed energy and power density on the divertor plates of ASDEX and ASDEX-Upgrade is described in this paper. Inertial cooled plates in the Divertor I of ASDEX as well as water-cooled plates in ASDEX-Upgrade and in the Divertor II of ASDEX are considered. In either case the temperature distribution on the surface of a representative divertor plate has to be measured with an appropriate space and time resolution as an input for the numerical computation. The time evolution of the profile of the surface temperature is determined with standard infrared measuring technique and details can be found in Refs. /1, 2, 3/.

Additional experimental information on the temperature profile of the rear side of the divertor plate are favourable and would considerably simplify the analysis but are not necessary in the case of actively cooled plates. The distribution of the absorbed energy and power density on the surface of the divertor plate is derived by solving the equation of heat conduction inside the plate with the measured profile of the surface temperature as a boundary condition.

A one-dimensional treatment of the heat conduction problem with constant thermophysical coefficients is justified in the large majority of the experimental situations /1/. Mostly, the component of the temperature gradient which is perpendicular to the surface of the plate exceeds the tangential components of the gradient by far and the elevation of the surface temperature is restricted to a few hundred degrees.

In part I of this paper the mathematical and numerical method is established. Principally, the absorbed energy density on a surface element as a function of time is directly computed by unfolding the measured surface temperature with an analytical function which is derived by Laplace-transformation technique from the equation of heat conduction. The absorbed power density is calculated from the energy density by a special numerical differentiation technique. The method is numerically stable and accurate. In part II some experimental data of ASDEX are analysed.

I. The Numerical Method

1) Inertial cooled divertor plate

The surface of the divertor plate is discretisized in arbitrary surface elements S_i. Each element S_i absorbs a power $P_i(t)$ and an energy $E_i(t)$ which are surface averaged values on the element S_i (Fig. 1). All the elements i are treated one-dimensionally in a first order approximation. Their thermo-physical properties are assumed to be constant and

the thermal coupling between the different elements is neglected. The cooling effect of the mounting supports of the plate is not considered.

Hence, $T_i(x,t)$ describes the temperature field in the element i and the course of $T_i(x,t)$ is described by

$$\frac{\partial^2}{\partial x^2}\delta_i(x,t) = \frac{c_p \cdot \varrho}{K}\frac{\partial}{\partial t}\delta_i(x,t) \tag{1}$$

$\delta_i(x,t) = T_i(x,t) - T_o$.

c_p is the heat capacity per unit mass, ϱ is the mass density and K is the thermal conductivity of the divertor plate.

We define the start of a heat pulse on the divertor plate at t = 0 and suppose the elapse of several heat diffusion times between the end of the previous heat pulse and the new pulse at t = 0.

The initial condition is then simply $T_i(x,0) = T_o$ or

$$\delta_i(x,0) = 0 \tag{2}$$

Inertial cooled plates means no cooling of the plate and the boundary conditions are

$$P(t) = -K\frac{\partial \delta_i}{\partial x}/_{x=0} \tag{3a}$$

$$\frac{\partial \delta_i}{\partial x}/_{x=d} = 0 \tag{3b}$$

In the following we omit the suffix i and denote $\delta(x,t)$ as temperature. The linear differential equation Eq. (1) with its initial condition Eq. (2) and its two boundary conditions Eqs. (3a) and (3b) can be solved analytically by Laplace-transformation technique. This method is well established and details can be found in standard text books /4,5/.

A function $f(x_1 ... x_K, t)$ can be represented by an integral in the complex plane s

$$f(x_1 ... x_K, t) = \frac{1}{2\pi j}\int_{a-j\infty}^{a+j\infty} F(x_1 ... x_K, s)e^{ts}ds$$

The function $F(x_1 ... x_K, s)$ is called the Laplace-transformed of $f(x_1 ... x_K, t)$

$$F(x_1 ... x_K, s) = L\{f(x_1 ... x_K, t)\} \tag{4a}$$

and the inverse transformation is defined as

$$f(x_1 ... x_K, t) = L^{-1}\{F(x_1 ... x_K, t)\} \tag{4b}$$

We use the notations of Eqs. (4a), (4b) throughout this paper.

Eq. (1) is Laplace-transformed to

$$\frac{\partial^2}{\partial x^2}\delta(x,s) = \frac{c_p \cdot \varrho}{K}[s \cdot \delta(x,s) - \delta(x,0)] \tag{5}$$

and simplified with the initial condition of Eq. (2) to

$$\frac{\partial^2}{\partial x^2}\delta(x,s) = \frac{c_p \cdot \varrho}{K} \cdot s \cdot \delta(x,s) \tag{6}$$

The Laplace-transformed boundary conditions are

$$P(s) = -K\frac{\partial\delta(x,s)}{\partial x}/_{x=0} \tag{7a}$$

$$0 = \frac{\partial\delta(x,s)}{\partial x}/x = d \tag{7b}$$

We find the general solution of Eq. (6) with the Ansatz $\delta(x,s) = c(s) \cdot e^{\lambda(s)\cdot x}$

$$\delta(x,s) = c_1(s)e^{\sqrt{\gamma}\sqrt{s}x} + c_2(s)e^{-\sqrt{\gamma}\sqrt{s}x} \tag{8}$$

and introduce the abreviation

$$\gamma = \frac{c_p \cdot \varrho}{K} \tag{9}$$

A straightforward derivation of $c_1(s)$ and $c_2(s)$ from Eq. (8) with the two boundary conditions Eqs. (7a), (7b) gives

$$c_1(s) = -\frac{P(s)}{K}\frac{1}{\sqrt{\gamma}\sqrt{s}} \cdot \frac{e^{-2\sqrt{\gamma}d\sqrt{s}}}{(e^{-2\sqrt{\gamma}d\sqrt{s}} - 1)} \tag{10}$$

$$c_2(s) = -\frac{P(s)}{K} \cdot \frac{1}{\sqrt{\gamma}\sqrt{s}} \cdot \frac{1}{(e^{-2\sqrt{\gamma}d\sqrt{s}} - 1)} \tag{11}$$

The Laplace-transformed of the surface temperature is $\delta(0,s) = c_1(s) + c_2(s)$ and with the notation $\beta = \sqrt{\gamma}d$ we find the solution for $\delta(0,s)$

$$\delta(0,s) = P(s) \cdot \sigma(s) \tag{12}$$

with

$$\sigma(s) = -\frac{1}{K\sqrt{\gamma}} \cdot \frac{1}{\sqrt{s}} \cdot \frac{(e^{-\beta\sqrt{s}} + e^{\beta\sqrt{s}})}{(e^{-\beta\sqrt{s}} - e^{\beta\sqrt{s}})} \tag{13}$$

Eq. (12) is transformed (L^{-1}) to the integral equation

$$\delta(0,t) = \int_0^t g(t-T) \cdot P(T) dT \tag{14}$$

with

$$g(t) = L^{-1}\{\sigma(s)\} = \frac{1}{2\pi j} \int_{a-j\infty}^{a+j\infty} \sigma(s) e^{ts} ds \tag{15}$$

The solution of the integral in Eq. (15) is found in the literature /6/ and Eq. (14) can be solved by inverting a triangular matrix. The elements of this matrix are defined by the values $g(t_n)$ taken at the various sample times $t_n (n = 1...N)$. In order to avoid the numerical problems which are inherent to the inversion of big triangular matrices (10^4 rows and columns respectively when 10^4 samples are taken for one surface element) we follow a different way of solving Eq. (12).

Instead of inverting a matrix we invert the complex function $\sigma(s)$ to $1/\sigma(s)$ and multiply the left and right side of Eq. (12) with 1/s.

$$\frac{1}{s} \cdot \frac{1}{\sigma(s)} \cdot \delta(0,s) = \frac{P(s)}{s} = W(s) \tag{16}$$

W(s) is the Laplace-transformed of the energy density W(t) which is absorbed on a surface element.

With the notation $F(s) = \frac{1}{\sigma(s)} \cdot \frac{1}{s}$ and $L^{-1}\{F(s)\} = F(t)$ we write the inverse-transformed Eq. (16) as

$$\int_0^t F(t-T) \cdot \delta(0,T) dT = W(t) \tag{17}$$

$$F(s) = K\sqrt{\gamma} \cdot \frac{1}{\sqrt{s}} \cdot tanh(\beta\sqrt{s}) \tag{17a}$$

and the inverse-transformed of F(s) is

$$F(t) = F_1(t) + F_2(t) = K\sqrt{\frac{\gamma}{\pi}} \cdot \frac{1}{\sqrt{t}} + 2K\sqrt{\frac{\gamma}{\pi}} \cdot \frac{1}{\sqrt{t}} \cdot \sum_{n=1}^{\infty} (-1)^n exp(-\frac{n^2\beta^2}{t}) \tag{18}$$

F(t) is composed of two parts. The first $F_1(t) = K\sqrt{\frac{\gamma}{\pi}} \cdot \frac{1}{\sqrt{t}}$ represents the solution for a infinitely thick plate $d \to \infty (\beta \to \infty)$ and has a singularity at r = 0. The second part $F_2(t) = K\sqrt{\frac{\gamma}{\pi}} \cdot \frac{1}{\sqrt{t}} \sum_{n=1}^{\infty} (-1)^n exp(-\frac{n^2\beta^2}{t})$ is contributed by the finite thickness d of the plate and shows no singularities.

The energy density W(t) is written as

$$W(t) = W_1(t) + W_2(t) = \int_0^t F_1(t-T)\delta(0,T)dT + \int_0^t F_2(t-T)\delta(0,T)dT \qquad (19)$$

Only the first part $W_1(t) = \int_o^t F_1(t-T)\delta(0,T)dT$ which is the exact solution for the thick plate is somewhat critical to compute and contains all the inherent numerical problems. Hence, we will only consider some experimental situations later on where $W_1(t)$ is dominant in order to show the applicability of the numerical method. It becomes now clearer why the factor 1/s is introduced in Eq. (16). The factor 1/s reduces the grade of the singularity at r = 0 and allows a stable and correct numerical solution of Eq. (16). A direct solution of Eq. (12) by inverting $P(s) = \delta(0,s)/\sigma(s)$ is much more difficult or even impossible. The measured surface temperature $\delta(0,t)$ is not smoothed at all and the raw data are used to solve Eq. (19).

2. The actively cooled divertor plate

In the case of an actively cooled divertor plate we have to introduce a physical model for the heat transport from the plate to the cooling medium. Normally the cooling medium is guided in tubes which are located at the rear or within the divertor plate and an effective thickness d of the plate has to be defined. The temperature of the cooling medium is measured at only one or at most a few positions on one divertor plate.

In section 2a we suppose an average temperature T_K of the cooling medium in one plate due to the lack of information. The application of the solution of 2a to any two-dimensional distribution of the temperature of the cooling medium in one plate is trivial. In section 2b we treat the special case where the temperature of the rear of the plate is known as a function of time.

2a) The temperature of the cooling medium is measured

The density of the heat flux within the plate at x = d is supposed to be proportional to the difference of the temperature of the cooling medium T_K and the temperature T(d,t) within the plate at x = d.

$$-K\frac{\partial T}{\partial x}/_{x=d} = \alpha[T(d,t) - T_K]$$

or

$$\frac{\partial \delta}{\partial x}/_{x=d} = -\frac{\alpha}{K}\delta(d,t) \qquad (20)$$

Eq. (7b) is replaced by

$$\frac{\partial}{\partial x}\delta(x,s)/_{x=d} = -\frac{\alpha}{K}\delta(d,s) \qquad (20b)$$

and Eq. (6) is solved in a similar way as is already described in section 1. The solution of Eq. (6) which corresponds to Eq. (16) is

$$W(s) = \delta(0,s) \cdot \sigma(s)$$

with

$$\sigma(s) = K\sqrt{\gamma} \cdot \frac{1}{\sqrt{s}} \cdot \frac{[(\sqrt{\gamma}\sqrt{s} + \frac{\alpha}{K})e^{\beta\sqrt{s}} - (\sqrt{\gamma}\sqrt{s} - \frac{\alpha}{K})e^{-\beta\sqrt{s}}]}{[(\sqrt{\gamma}\sqrt{s} + \frac{\alpha}{K})e^{\beta\sqrt{s}} + (\sqrt{\gamma}\sqrt{s} - \frac{\alpha}{K})e^{-\beta\sqrt{s}}]} \tag{21}$$

In order to find the inverse-transformed of $\sigma(s)$ we have to solve the integral

$$\sigma(t) = \frac{1}{2\pi j}\int_{a-i\infty}^{a+i\infty} \sigma(s)e^{ts}ds \tag{22}$$

$\sigma(s)$ is uniquely defined in the complex plane s due to $[r \cdot e^{i(\varphi+2\pi)}]^{1/2} = -[re^{i\varphi}]^{1/2}$ and hence $\sigma(re^{i(\varphi+2\pi)}) = \sigma(re^{i\varphi})$.

For $s \to \infty \quad \sigma(s) \to K\sqrt{\gamma}\frac{1}{\sqrt{s}} \cdot tanh(\beta\sqrt{s})$ and this proves that $\sigma(t)$ is represented by the sum of the residua of $\sigma(s) \cdot e^{ts}$.

The non-trivial poles of $\sigma(s)$ are derived from

$$e^{-2\beta\sqrt{s}} = -\frac{(\sqrt{\gamma}\sqrt{s} + \frac{\alpha}{K})}{(\sqrt{\gamma}\sqrt{s} - \frac{\alpha}{K})} \tag{23}$$

with the Ansatz $s = -A^2 \quad (A > 0)$.

We find the single poles of $\sigma(s)e^{ts}$ at

$$s = 0$$

with the residuum

$$Res(0) = \frac{\varepsilon}{(1 + \varepsilon\beta)} \tag{24}$$

and at

$$s_n = -A_n^2 = -\frac{\pi^2}{\beta^2}(n - \frac{1}{2})^2 - g_n(\alpha) \qquad (n = 1,2,3....\infty) \tag{25}$$

with the residua

$$Res(s_n) = \frac{2(A_n^2 + \varepsilon^2)}{\varepsilon + \beta(A_n^2 + \varepsilon^2)}e^{-A_n^2 \cdot t} \tag{26}$$

and use the notations $\beta = \sqrt{\gamma}d$ and $\varepsilon = \frac{\alpha}{K\sqrt{\gamma}}$.

$g_n(\alpha)$ is derived from the equation

$$cos(2\beta A_n) = -\frac{(A_n^2 - \varepsilon^2)}{(A_n^2 + \varepsilon^2)} \tag{27}$$

by using Newton's iteration technique and with the constraint $(n+\frac{1}{2})\frac{\pi}{\beta} \leq A_n \leq (n+1)\frac{\pi}{\beta}$.

The general unfolding function $\sigma(t)$ for the actively cooled plate of thickness d is

$$\sigma(t) = \frac{\varepsilon}{(1+\varepsilon\beta)} + 2 \cdot \sum_{n=1}^{\infty} \frac{(A_n^2+\varepsilon^2)}{[\varepsilon+\beta(A_n^2+\varepsilon^2)]} \cdot e^{-A_n^2 \cdot t} \tag{28}$$

Without cooling ($\alpha = 0$) $\sigma(t)$ simplifies to

$$\sigma(t) = \frac{2}{\beta} \cdot \sum_{n=1}^{\infty} exp[-\frac{\pi^2}{\beta^2}(n-\frac{1}{2})^2 \cdot t] \tag{29}$$

and is proven to be identical with F(t) of Eq. (18).

The unfolding functions for the thick plate $F_1(t)$, for the thin plate $F(t)$ and for the cooled plate $\sigma(t)$ are compared in Fig. 2 for copper as the plate material. $F(t)$ and $\sigma(t)$ describe the uncooled and cooled divertor plates of the Divertor II in ASDEX with data taken from Ref. /7/.

For $t \leq 0.1\beta^2$ the deviation of either $F(t)$ and $\sigma(t)$ from the thick plate solution $F_1(t)$ is less than $2 \cdot 10^{-4}$. Hence, the absorbed energy density on the thick plate and on the cooled and uncooled plate is described by the same expression

$$W(t) = \int_0^t F_1(t-T) \cdot \delta(0,T)dT \quad (t \leq 0.1\beta^2) \tag{30}$$

For $t > 0.1\beta^2$ we have to replace $F_1(t)$ by the proper unfolding function $F_1(t), F(t)$ and $\sigma(t)$ in order to solve Eq. (30).

The variation of the positions of the first four poles S_1, S_2, S_3 and S_4 with the parameter $\alpha d/\pi K$ is shown in Fig. 3. A pronounced variation is observed for $0.3 \lesssim \alpha d/\pi K \lesssim 10$ and the calibration of the thermographic diagnostics concerning the parameter α has to be performed by fitting the calculated energy density to the course of a test pulse.

The measured raw data of the surface temperature $\delta(0,t_1), \delta(0,t_2) ... \delta(0,t_N)$ are linearly interpolated between the samples taken and the integral in Eq. (30) is analytically evaluated. This technique yields much better results than a purely numerical integration. The analysis techniques of section 1 and 2a are sufficient for the thermographic diagnostics and were exclusively used to analyse ASDEX data.

2b) The temperatures at the front and rear of the plate are measured

Usually, the temperature distribution at the rear of the plate is not accessible. But in order to complete the analysis of the cooled plate we shortly treat this special case which considerably simplifies the analysis.

The boundary condition of Eq. (20b) simplifies to

$$H(s) = -\frac{\alpha}{K}\delta(d,s) = \frac{\partial}{\partial x}\delta(x,s)/_{x=d} \tag{31}$$

where the function H(s) is known and we get the Laplace-transformed of the energy density

$$W(s) = \delta(0,s)F(s) - 2K\frac{H(s)}{[e^{\beta\sqrt{s}} + e^{-\beta\sqrt{s}}]\cdot s} \tag{32}$$

The solution of Eq. (32) is

$$W(t) = \int_0^t F(t-T)\delta(0,T)dT - K\int_0^t A(t-T)H(T)dT \tag{33}$$

with

$$A(t) = 1 - \frac{4}{\pi}\sum_{n=0}^{\infty}\frac{(-1)^n}{(2n+1)}exp[-\frac{\pi^2}{\beta^2}(n+\frac{1}{2})^2\cdot t]$$

and the integrals of Eq. (33) are analytically solved as is described in section 2a. F(t) is given by Eq. (18).

The main advantage of this method is the simple calibration of the diagnostics with regard to α. Only $H(t) = -\frac{\alpha}{K}\delta(d,t)$ depends on α while the poles s_n are independent on α.

3. Derivation of the Absorbed Power Density P(t) from W(t)

The power density P(t) is derived from the energy density W(t) by differentiating the computed W(t). In order to avoid the numerical problems which are inherent to the various differentiation methods we tackel the problem differently.

The surface temperature of each plate element is sampled with a frequency f_s. In order to eliminate aliasing effects a limitation of the bandwidth of the measured signal to $f_s/2$ is demanded by the Nyquist theorem before sampling.

We introduce a mathematical filter function $SM(t,f_g)$ with a 3-db bandwidth $f_g \leq f_s$ and process the sampled raw data W(t) with the filter function $SM(t,f_g)$ like

$$W_s(t,f_g) = \int_0^t SM(t-T,f_g)W(T)dT \tag{34}.$$

There will be no loss of information in $W_s(t,f_g)$ compared to W(t) if $f_g \geq f_s/2$. With $f_g < f_s/2$ the function $W_s(t,f_g)$ represents the smoothed energy density W(t).

A similar integral relation is valid for the n-times differentiated energy density $W^{(n)}(t)$

$$W_s^{(n)}(t,f_g) = \int_0^t SM(t-T,f_g)W^{(n)}(T)dT = \int_0^t SM^{(n)}(t-T,f_g)W(T)dT \tag{35}$$

The differentiation is swopped from the processed function W(t) to the filter function $SM(t, f_g)$. A prove of Eq. (35) can be performed by using Laplace-transformation technique.

We choose a filter function which can be represented in an analytical form. This allows the n-times differentiation of W(t) to be performed by a n-times analytical differentiation of the filter function $SM(t, f_g)$ and then unfolding W(t) with $SM^{(n)}(t, f_g)$. $SM(t, f_g)$ and its derivatives have to be calculated once and are then filed in a table.

W(t) is only smoothed if n = 0 and $f_g < f_s/2$. Smoothing and additional n-times differentiation of W(t) is performed with $n \geq 1$ and $f_g < f_s/2$. Good results are obtained with a filter function which corresponds to a Bessel-filter. These so-called "minimum phase shift" filters show a constant group velocity and an optimum response to pulsed functions.

The filter function is represented by a sum

$$SM(t, f_g) = a(f_g) \cdot \sum_{i=1}^{N} e^{b_i(f_g) \cdot t} [c_i(f_g) cos(d_i(f_g) \cdot t) + e_i(f_g) sin(f_i(f_g) \cdot t)] \qquad (36)$$

$SM(t, f_g)$ and $SM^{(1)}(t, f_g)$ are shown in Fig. 4 for a sample frequency $f_s = 1$ KHz, a bandwidth $f_g = 500Hz$ and the index N = 5 (10-pole Bessel-filter).

$W_s^{(n)}(t, f_g)$ is calculated at each sample time (Eq. (35)) with a very limited number of multiplications. M = 7 multiplications are necessary in order to evaluate $W_s(t, f_g)$ for $f_g = 500Hz$, N = 5 and M = 16 multiplications for $W_s^{(1)}(t, f_g)$. This follows from the shape of the filter functions in Fig. 4. The presented differentiation and smoothing technique is accurate, stable and has no numerical problems at all.

II. Results

1. Test of the numerical method

The numerical method is tested for the thick plate with a simulated function for the absorbed power density P(t). We assume that the test power density is switched on from zero to 1 W/m^2 at t = 0 and remains then constant. Eq. (1) predicts the elevation of the surface temperature in response to the power test function as $\delta(0, t) = 2\sqrt{t}/(\sqrt{\pi\gamma}K)$. N samples are taken from $\delta(0, t)$ at times $t_n = (n-1) \cdot 10^{-3}s$ (n = 1... N) with a sample frequency $f_s = 1$ KHz. The set of N samples $\delta(0, t_n)$ represents the 'measured' test surface temperature. We retrieve the energy density from $\{\delta(0, t_n)\}$ with

$$W(t_n) = K\sqrt{\frac{\gamma}{\pi}} \int_0^{t_n} \frac{1}{\sqrt{t-T}} \delta(0, T) dT \qquad (37)$$

and the test power density with

$$P(t_n, f_g) = \int_0^{t_n} SM^{(1)}(t - T, f_g) W(T) dT \qquad (38)$$

$P(t_n, f_g)$ is computed with the Simpson formula which yields sufficient good results. Fig. 5 compares the test power density with the result of the computation $\{P(t_n, f_g)\}$ without smoothing (f_g = 500 Hz).

A small overswing at the beginning and a small drift of the computed power density is observed at full bandwidth. The drift can probably be reduced further by introducing an improved integration method for the unfolding integral in Eq. (38) similar to the method which is already described in section 2a for the integral in Eq. (37). Smoothing reduces the drift and almost completely eliminates the overswinging. Fig. 6 shows the result with strong smoothing (f_g = 30 Hz) and unveils a delay time $\tau_D(f_g)$ of the filter function which has to be considered in Eq. (38). The corrected formula for the power density is

$$P(t_n - \tau_D(f_g), f_g) = \int_0^{t_n} SM^{(1)}(t - T, f_g) W(T) dT \qquad (39)$$

and is exclusively used for the analysis of ASDEX data.

An analytical formula supplies the delay times for the various bandwidths and $\tau_D(f_g)$ is filed in a table, too.

2. Analysis of experimental ASDEX data

In order to demonstrate the applicability of the numerical method on experimental data of the ASDEX thermographic diagnostics we analyse the measured surface temperature of one plate element S_i. Profiles of the power density on the divertor plates of ASDEX and parameter studies of the total deposited power will be published elsewhere.

Three examples for the divertor I of ASDEX with 0.2 cm thick titanium plates are presented. Fig. 7a shows the measured temperature elevation of the representative surface element during neutral beam injection with P_{NBI} = 1.7 MW and ion cyclotron resonance heating with P_{ICRH} = 1.7 MW for the discharge # 16080. The duration of the heating pulse Δt = 0.6 s is somewhat shorter than the heat diffusion time $\tau_D = \beta^2/2 = 0.7s$. It follows from Fig. 2 that the 'thick plate' approximation is useful. A nearly linear rise of the absorbed energy density with time is deduced from Fig. 7b. Small oscillations indicate the presence of sawteeth. This becomes more obvious in Fig. 7c where the power density is represented. Good agreement of the calculated power density with the result of a different computational technique /1/ is obtained but the new method is much faster. A reduction in CPU-time of at least 10 was estimated for the new method.

Another neutral-beam heated discharge (# 16084) with P_{NBI} = 1.7 MW and P_{ICRH} = 1.2 MW is shown in Figs. 8a, 8b and 8c, but with a shorter duration of the heating pulse. A sample frequency of 250 Hz is used in either example. The drift of the power density after switching off the heating is proved to be not a numerical error but seems to be a drift of the thermographic diagnostics. Very high power densities are deposited on the divertor plates during a disruption (# 15779). A temperature rise of several

hundred degrees in a few milliseconds is observed in Fig. 9a. This results in a step-like elevation of the energy density (Fig. 9b) and a huge spike in the power density up to 500 W/cm^2. But the maximum power density is probably much higher and its real value is masked by the relatively low sampling rate of 250 Hz.

Conclusions

A fast and simple numerical method is presented which computes the absorbed power density on surfaces of solids from the measured surface temperature alone. A one-dimensional description with constant thermophysical coefficients has been used which covers most of the experimental situations for the divertor plates in ASDEX and ASDEX-Upgrade. The method is useful for all kinds of inertial cooled and actively cooled plates and comprises two computational steps.

First, the absorbed energy density on the plate is computed by unfolding the measured raw data of the surface temperature with an analytical function which is derived by solving the equation of heat conduction with Laplace-transformation technique.

In the second step the power density is calculated by differentiating the energy density with an unfolding technique. This method of differentiation is numerically stable and allows for differentiating and smoothing in one step. An analytical unfolding function which simulates a 10-pole Bessel filter yields good results and needs only the 3-db bandwidth as an input. Compared to differentiating techniques which fit splines or other functions into the raw data there does not exist any possibility of falsification of the physical information which is inherent to the signal. Good agreement was obtained between the results which are derived with the new computation method and a previous technique /1/ which is already mentioned in this report. A CPU-time of 28 seconds is needed on an IBM 3090 computer in order to calculate the power density on 50 surface elements at 1000 sample times each.

Acknowledgements

The authors would like to thank M. Harnau for transmitting the data files and Ch. Röder for preparing the manuscript.

References

1) B.K. Bein, E.R. Müller, J. of Nucl. Mat. 111 + 112 (1982) 548.

2) T. Hino et al., J. of Nucl. Mat. 121 (1984).

3) D.N. Hill et al., Nucl. Fusion 28, No. 5 (1988).

4) G. Doetsch, Theorie der Laplace-Transformation, Verlag Birkhäuser, Basel.

5) H.S. Carlslaw and J.C. Jaeger, Conduction of heat in solids, Oxford Univ. Press London 1973.

6) F. Oberhettinger, L. Badii, Tables of Laplace Transformation, Springer Verlag 1973.

7) H. Würz, B.K. Bein et al., to be published in the Proceedings of the 15th SOFT Conference, Utrecht, Sept. 1988.

Figure Captions

Fig. 1

a) Schematic view of a discretisized plate.

b) $T_i(x,t)$ = temperature distribution across the plate of thickness d at time slice t. T_o = const (x) = initial temperature profile.

Fig. 2 Comparison of the unfolding functions for a 8 mm thick copper plate in the divertor II in ASDEX.

Fig. 3 Positions of the first 4 poles on the negativ real axis in the complex plane s.

Fig. 4

a) Analytical unfolding function SM(t, f_g) for exclusively smoothing (10-pole Bessel filter). The sample frequency is f_s = 1 KHz and the 3-db bandwidth f_g = 500 Hz.

b) Representation of $SM^{(1)}(t, f_g) = \frac{\partial}{\partial t} SM(t, f_g)$. The differentiation of SM(t, f_g) in Fig. 4a is performed analytically.

Fig. 5 Comparison of the test power pulse P(t) = 1 W/m^2 (t > 0) and the result of the computation without smoothing.

Fig. 6 Test power pulse and computed power density with strong smoothing (f_g = 30 Hz).

Fig. 7

a) Measured surface temperature

b) Computed energy density

c) Computed power density during neutral beam injection for # 16080 in ASDEX.

Fig. 8

a) Measured surface temperature

b) Computed energy density

c) Computed power density during neutral beam injection for # 16084 in ASDEX.

Fig. 9

a) Measured surface temperature

b) Computed energy density

c) Computed power density for an ASDEX discharge which is terminated by a disruption.

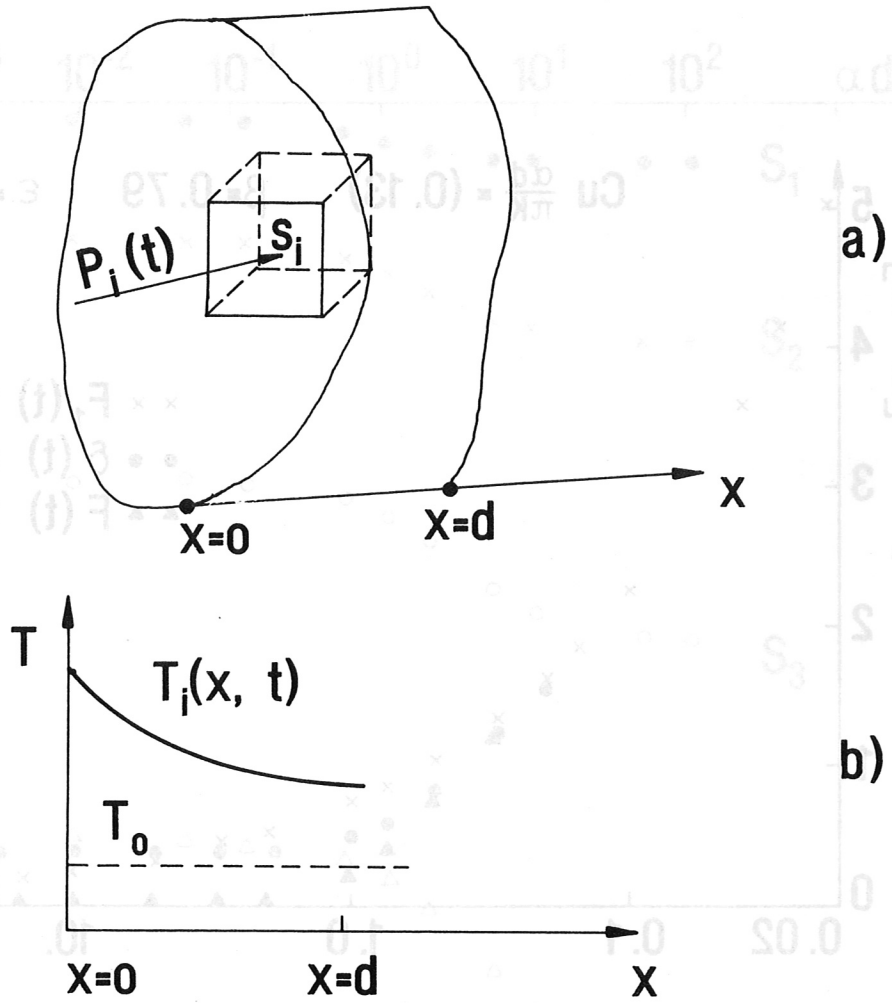

Fig. 1: a) Schematic representation of a discretisized plate
b) $T_i(x, t)$ = temperature distribution across the plate of thickness d at the time t. T_0 = const = initial temperature profile. $P_i(t)$ = power density on the plate.

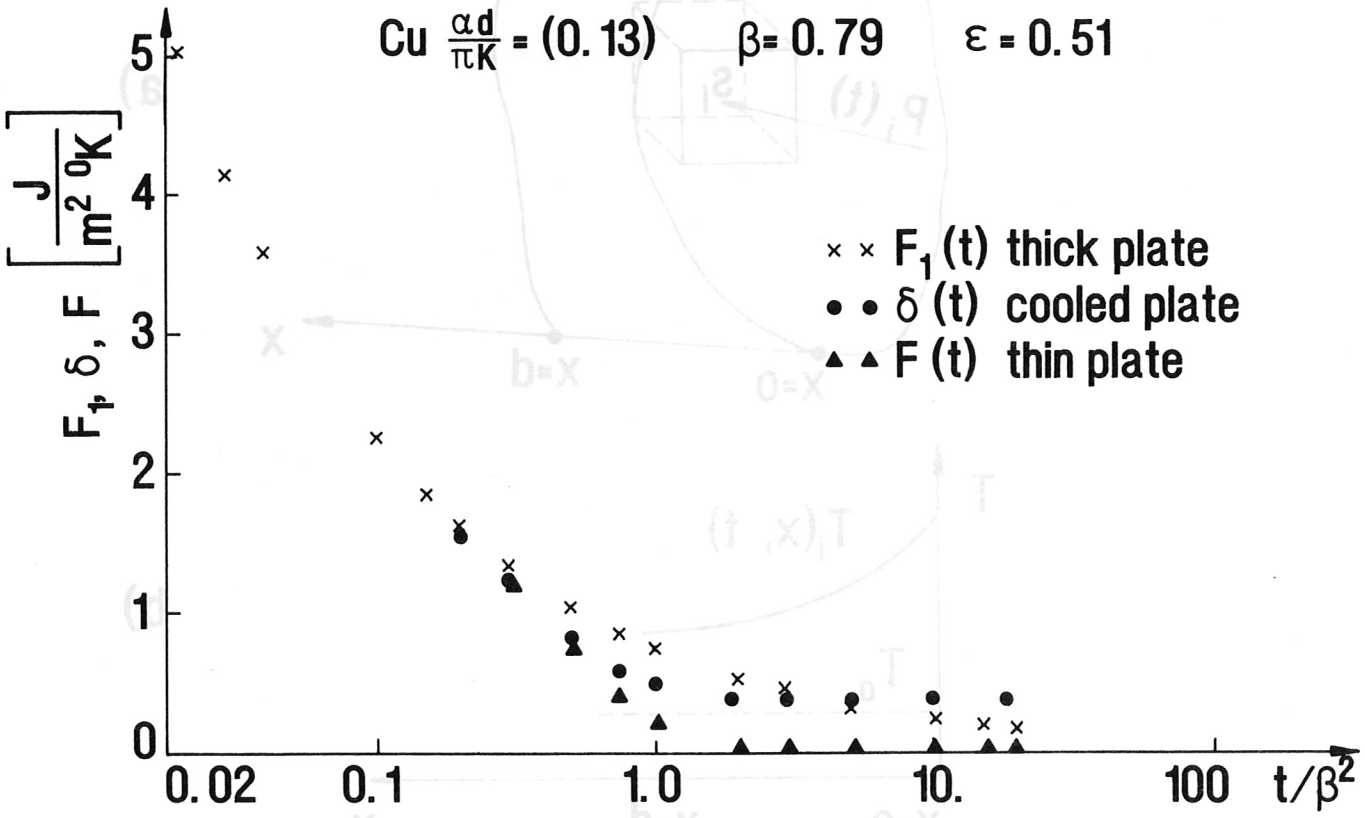

Fig. 2: Comparison of the unfolding functions for a 8mm thick copper plate in the divertor II in ASDEX. The three curves for $t/\beta^2 < 0.4$ are falling together in one curve.

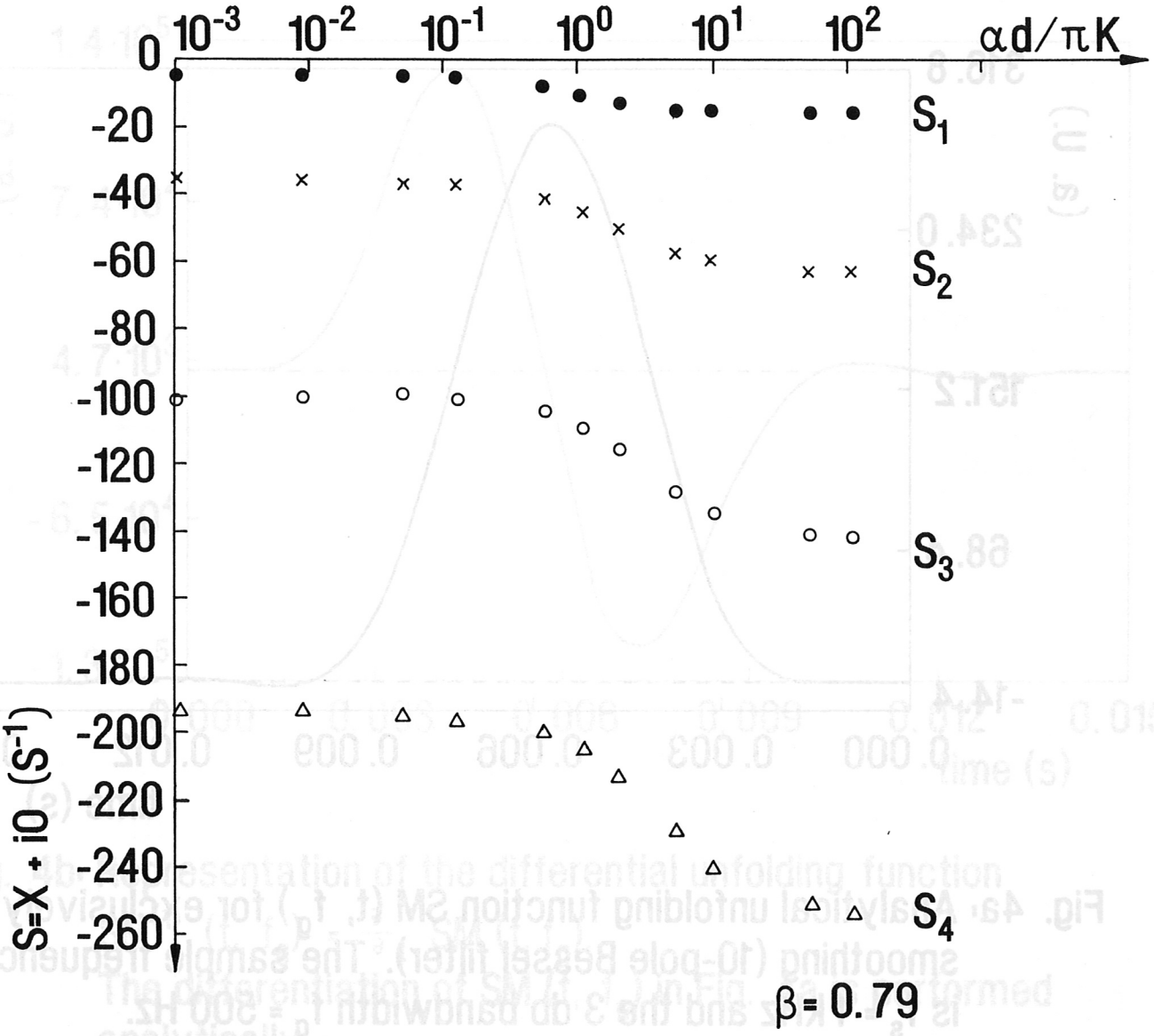

Fig. 3: Positions of the first 4 poles on the negativ real axis in the complex plane S.

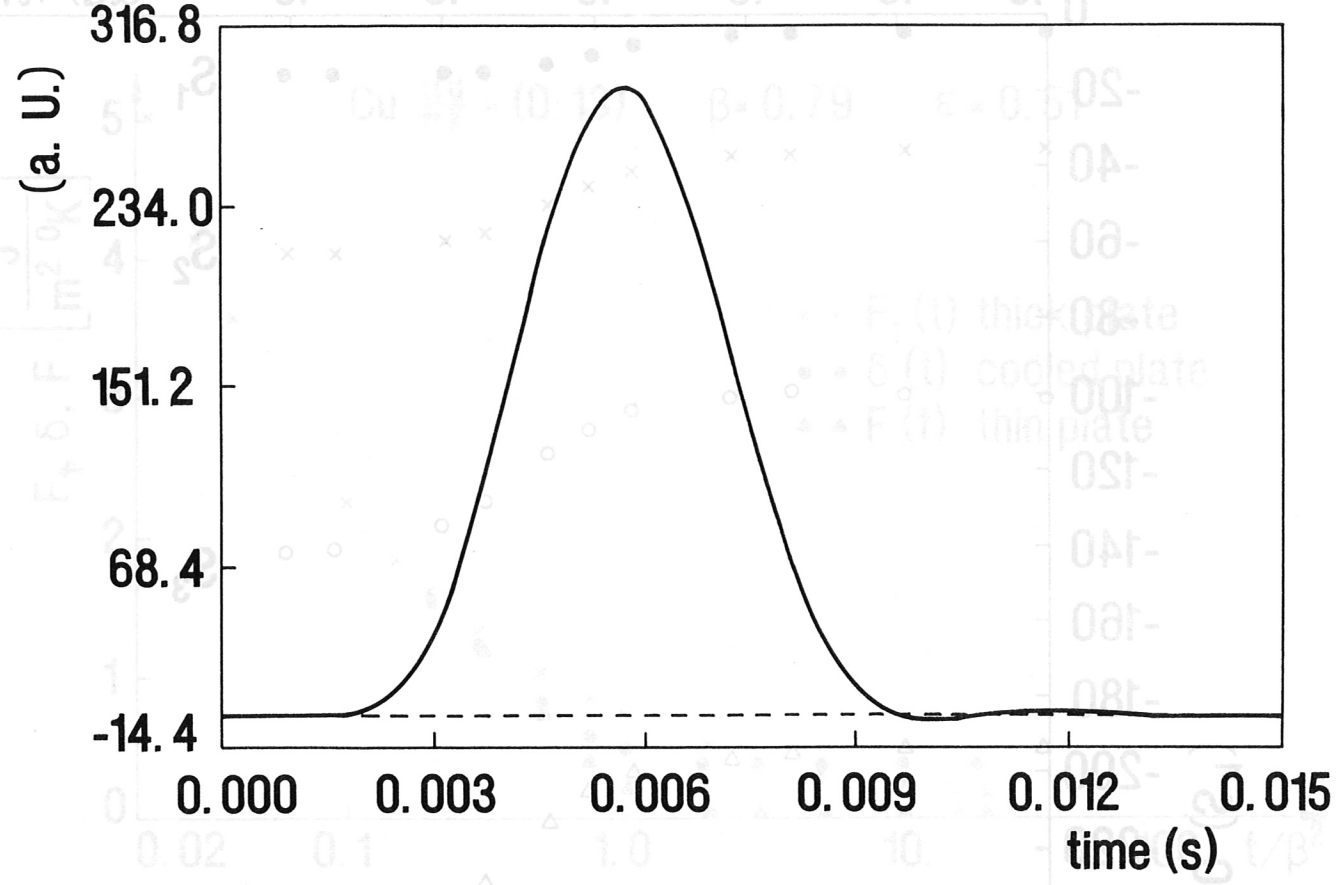

Fig. 4a: Analytical unfolding function SM (t, f_g) for exclusively smoothing (10-pole Bessel filter). The sample frequency is f_s = 1 kHz and the 3 db bandwidth f_g = 500 Hz.

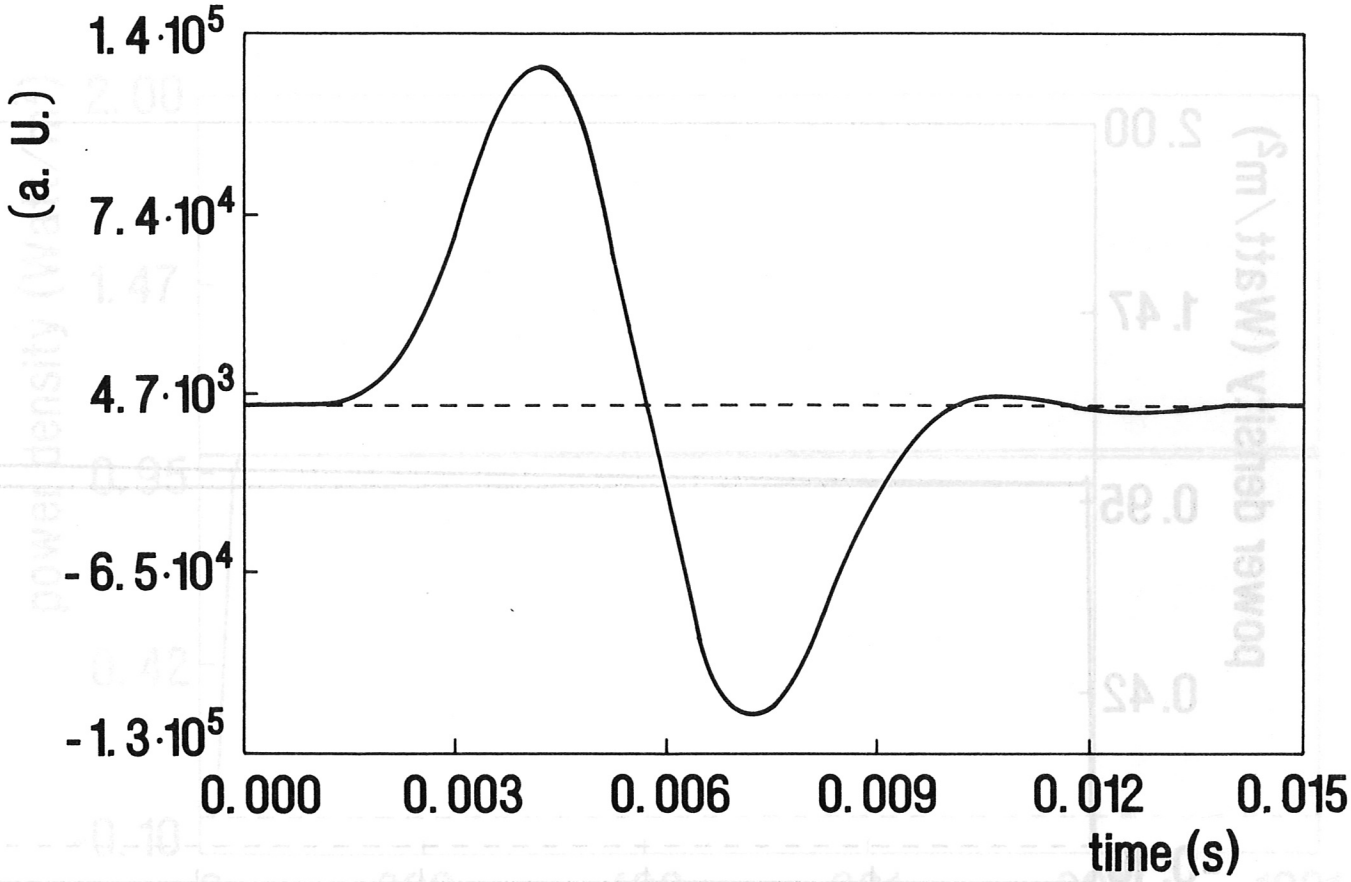

Fig. 4b: Representation of the differential unfolding function $SM^{(1)}(t, f_g) = \frac{\partial}{\partial t} SM(t, f_g)$.
The differentiation of $SM(t, f_g)$ in Fig. 4a is performed analytically.

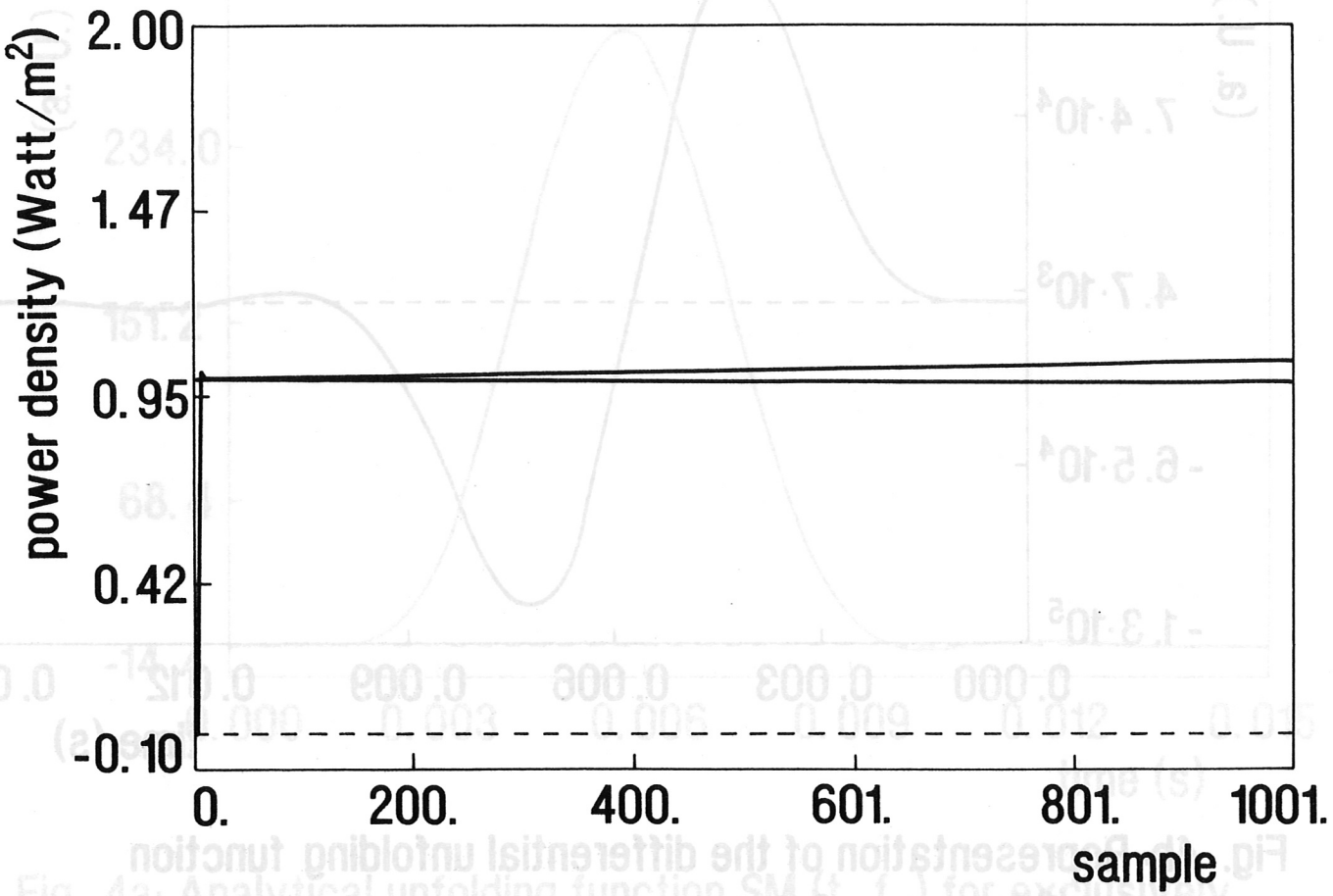

Fig. 5: Comparison of the test power pulse $P(t)=1W/m^2$ $(t>o)$ and the result of the computation without smoothing

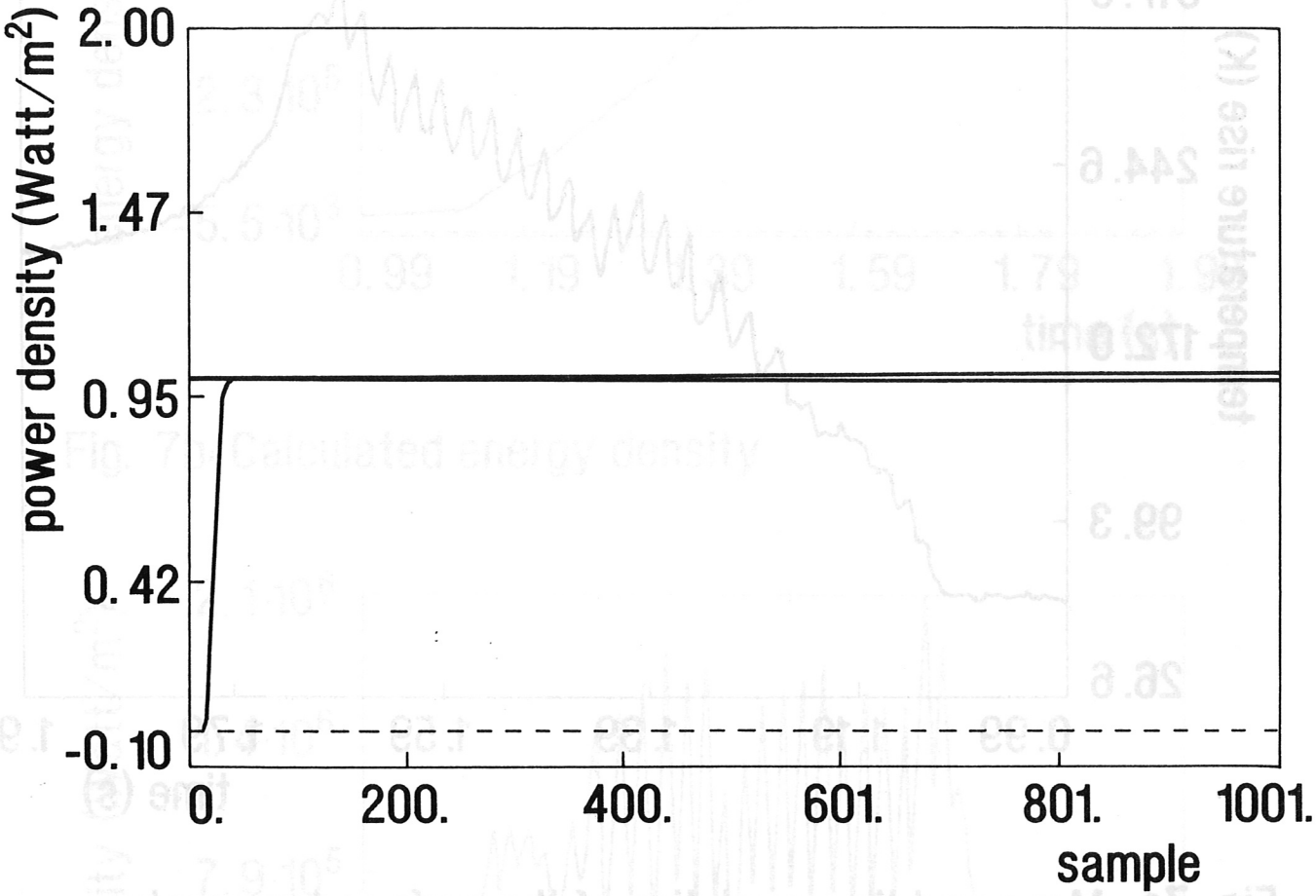

Fig. 6: Test power pulse and computed power density with strong smoothing (f_g=30 Hz)

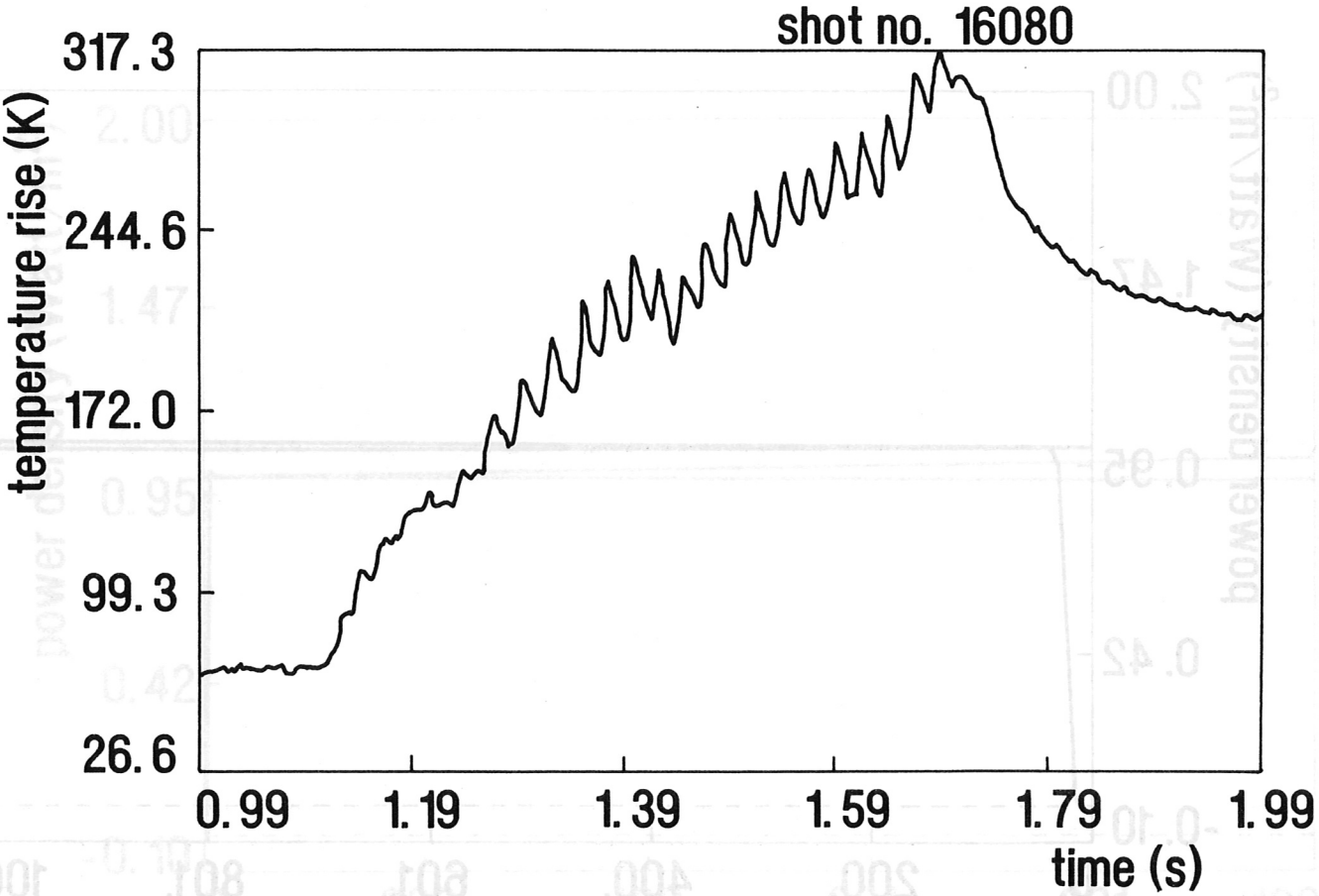

Fig. 7a: Measured time evolution of the surface temperature during neutral beam heating in ASDEX

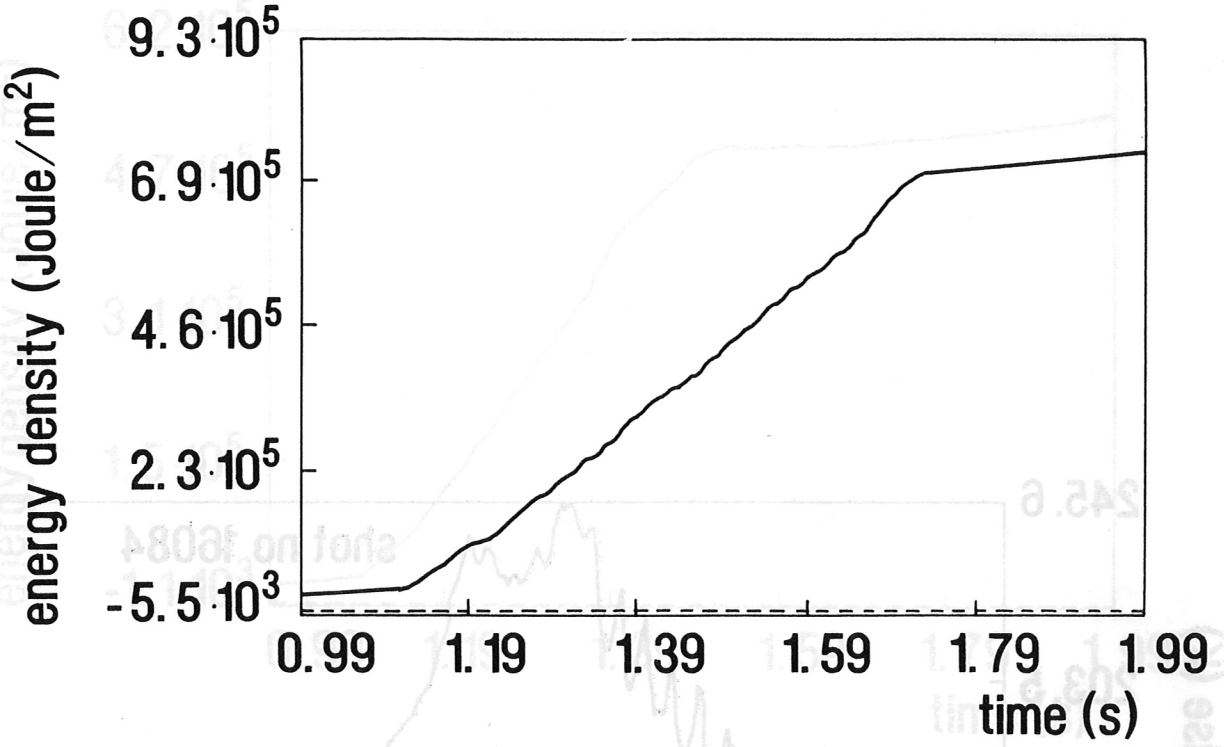

Fig. 7b: Calculated energy density

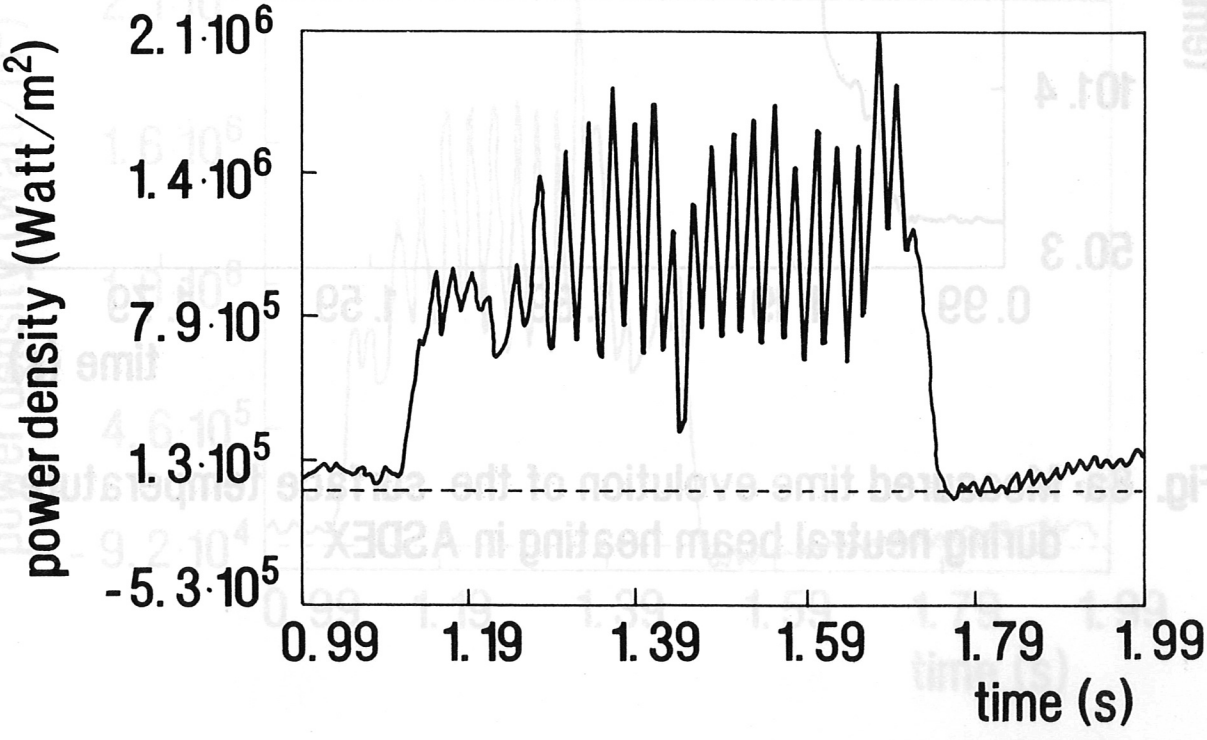

Fig. 7c: Calculated power density during neutral beam injection for shot no 16080 in ASDEX

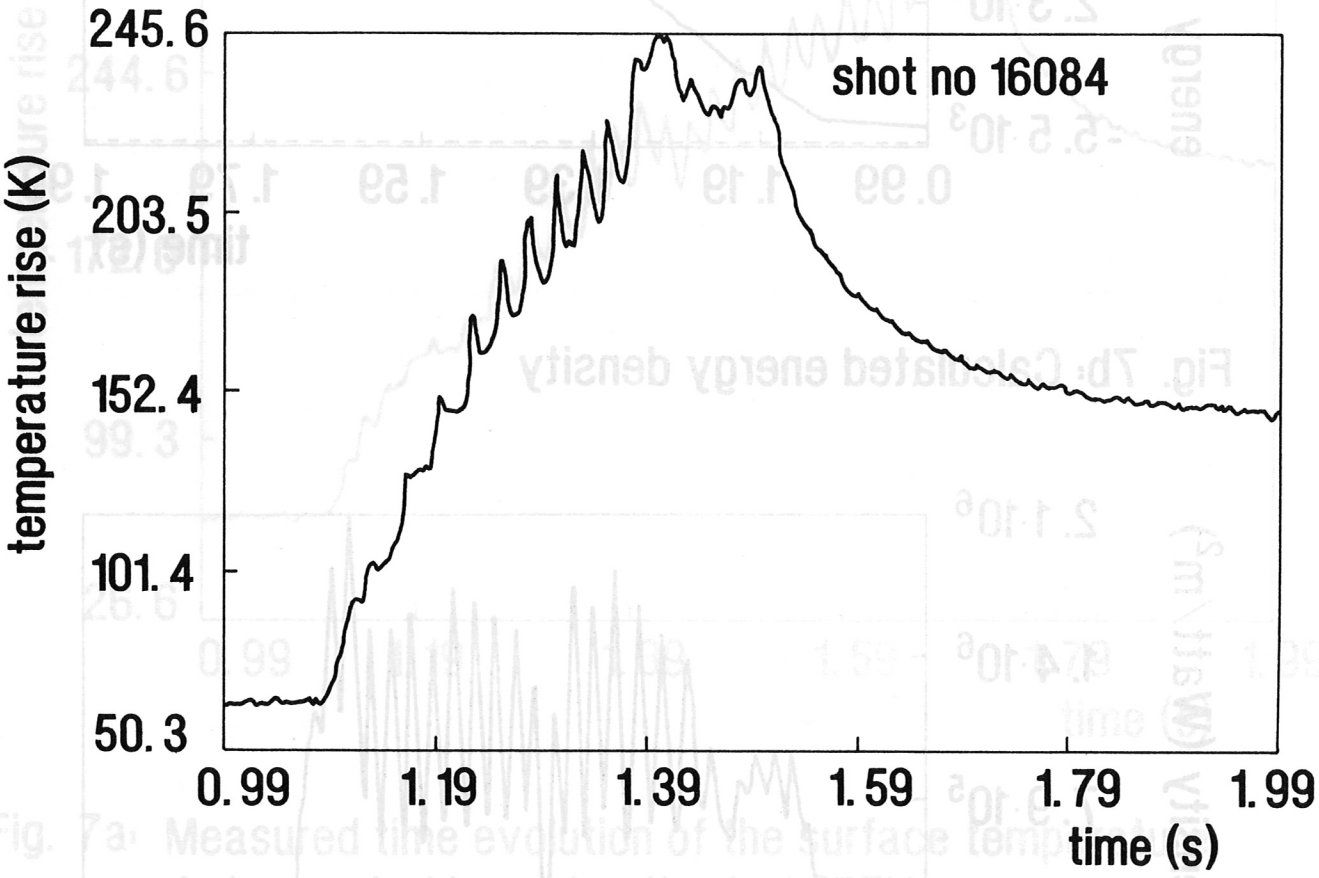

Fig. 8a: Measured time evolution of the surface temperature during neutral beam heating in ASDEX

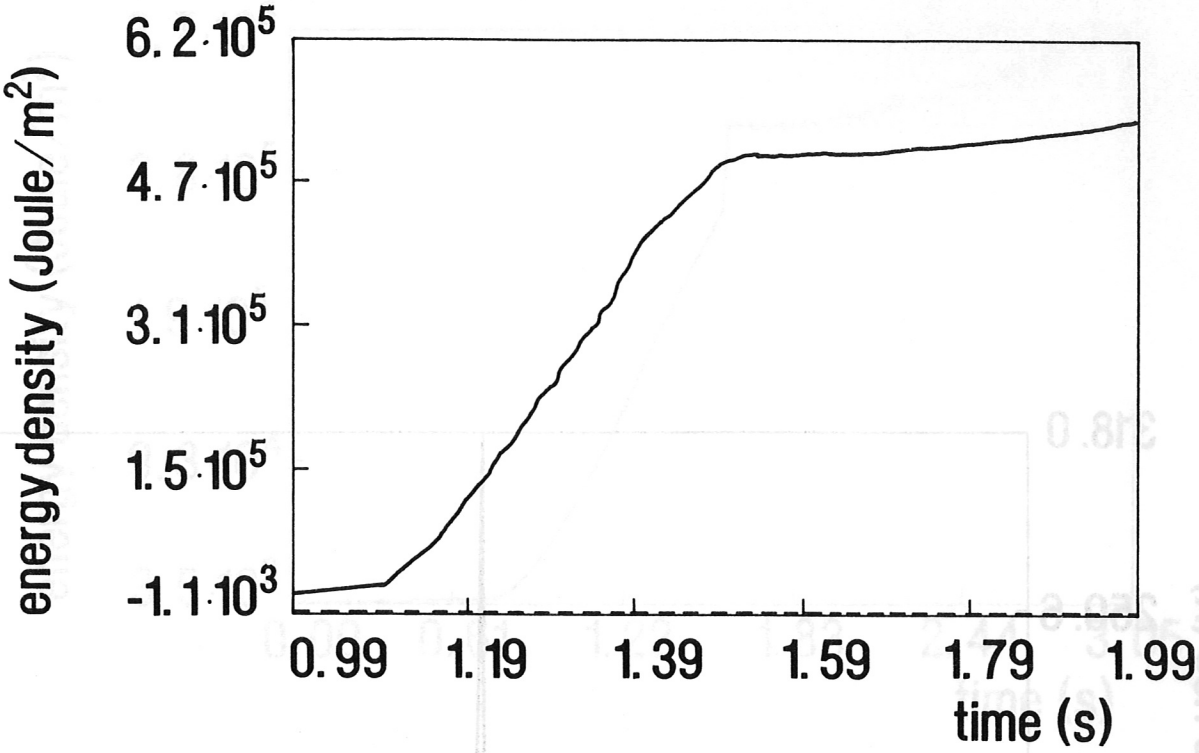

Fig. 8b: Calculated energy density

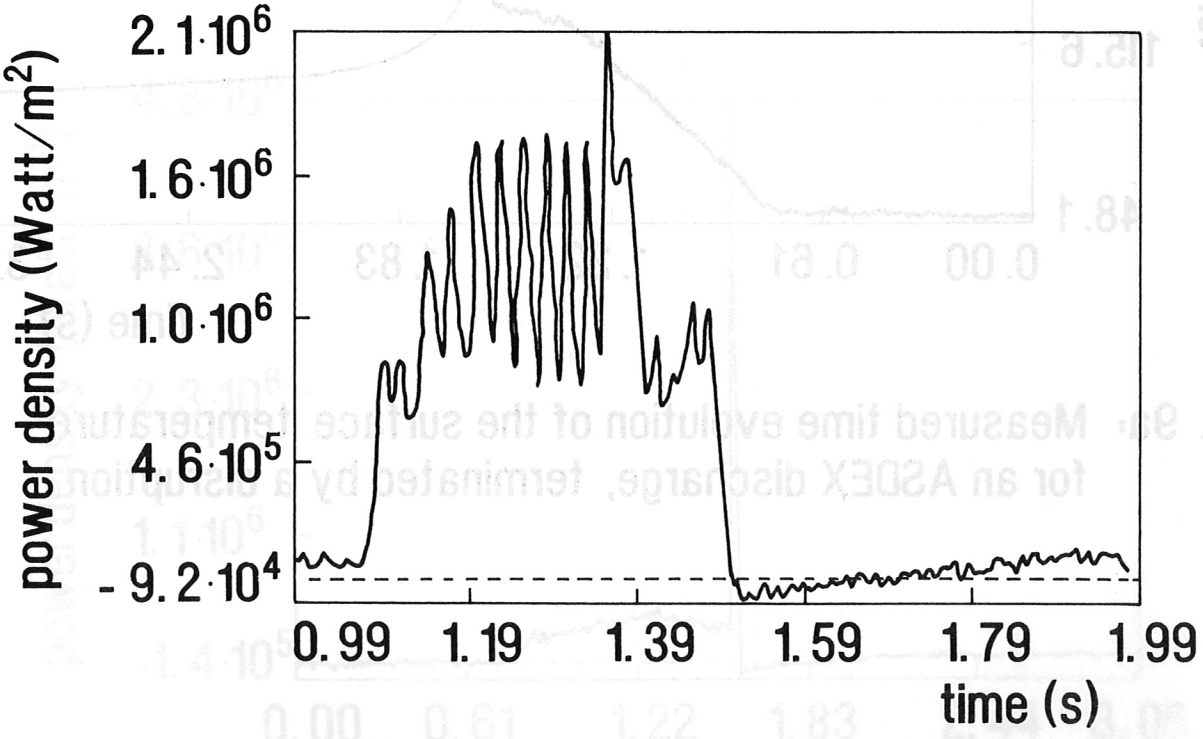

Fig. 8c: Calculated power density during neutral beam injection for shot no 16084 in ASDEX

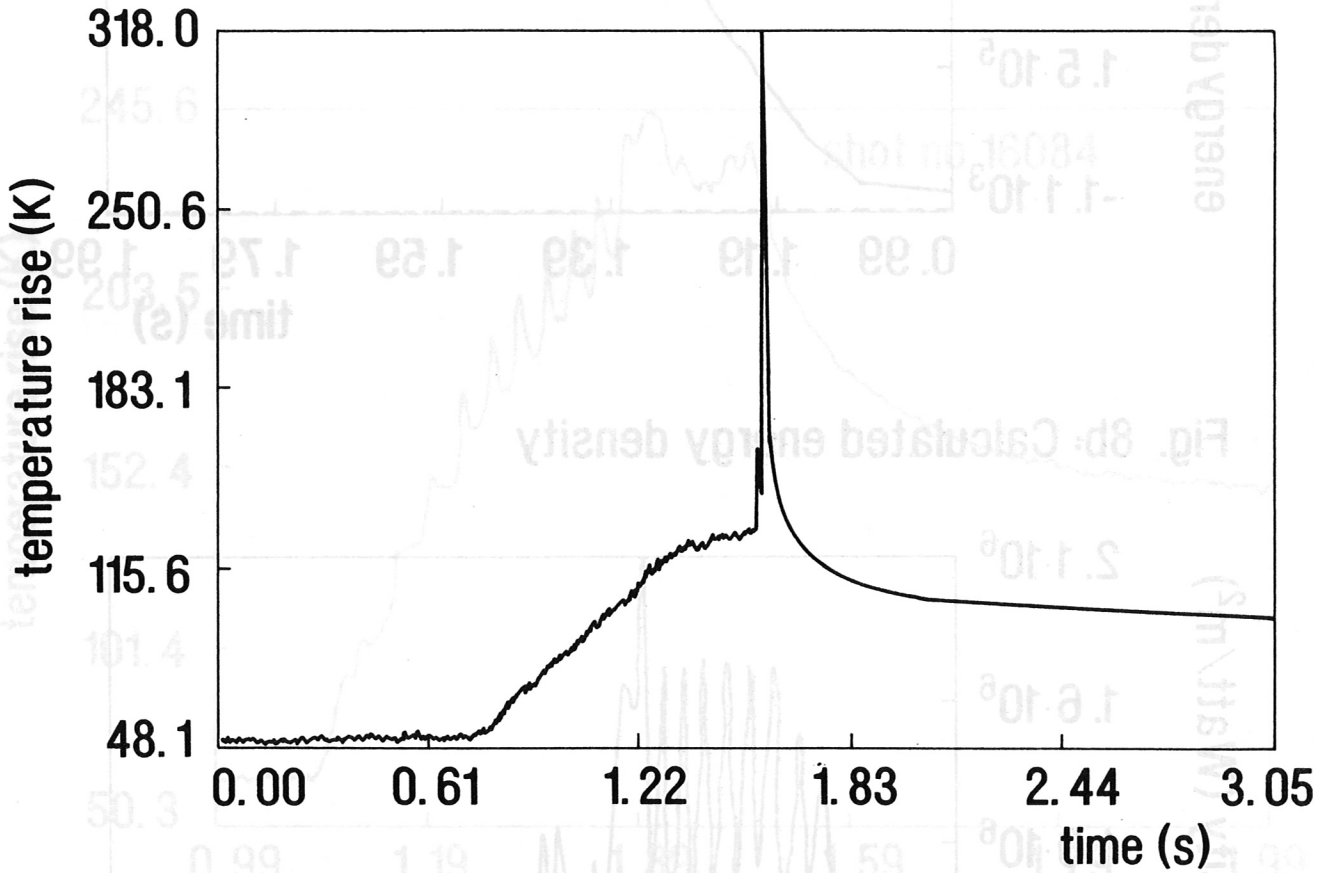

Fig. 9a: Measured time evolution of the surface temperature for an ASDEX discharge, terminated by a disruption

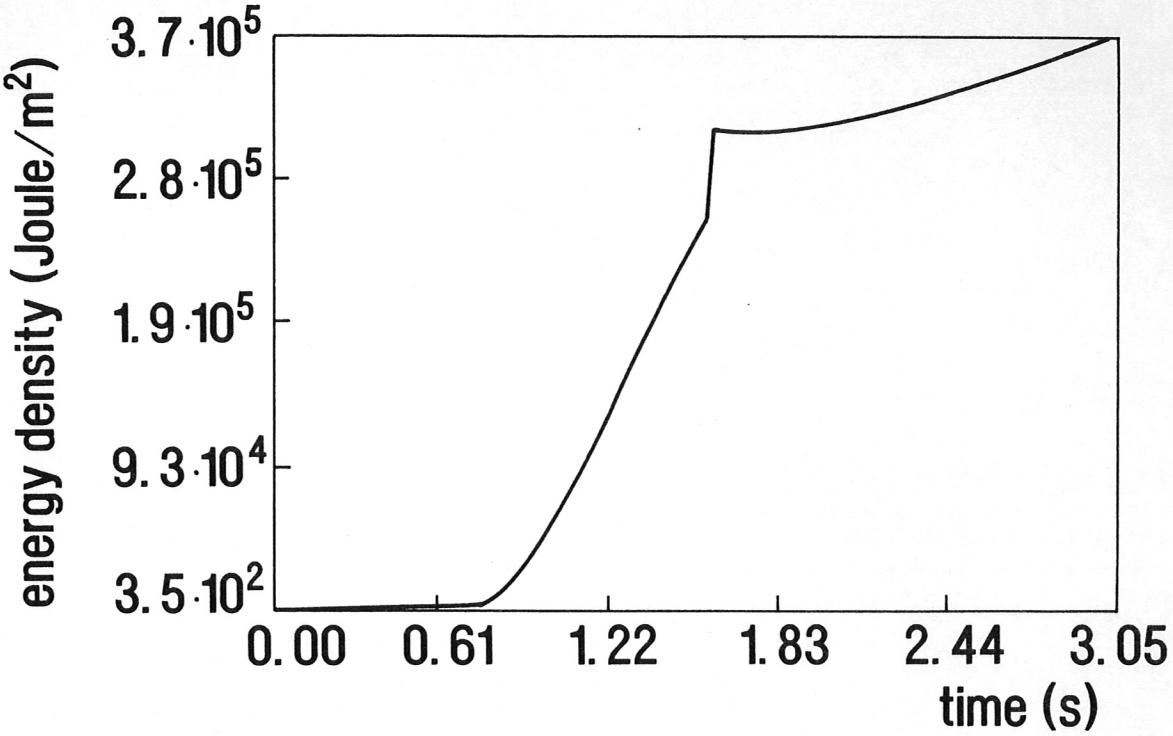

Fig. 9b: Calculated energy density

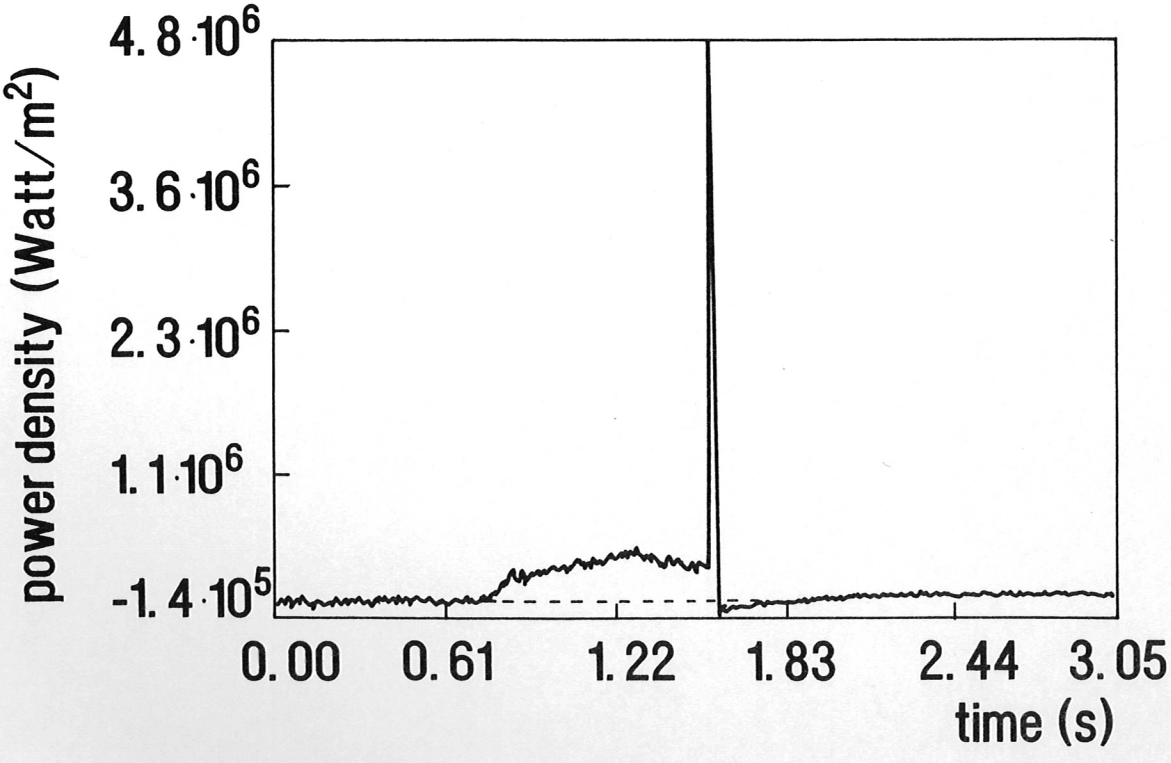

Fig. 9c: Calculated power density for an ASDEX discharge which terminated by a disruption